Supporting Information

Photoluminescence Segmentation within Individual Hexagonal Monolayer Tungsten Disulfide Domains Grown by Chemical Vapor Deposition

Yuewen Sheng[1], Xiaochen Wang[1], Kazunori Fujisawa[2], Siqi Ying[3], Ana L. Elias[2], Zhong Lin[2], Wenshuo Xu[1], Yingqiu Zhou[1], Alexander M. Korsunsky[3], Harish Bhaskaran[1], Mauricio Terrones[2,4], Jamie H. Warner[1]*

[1]Department of Materials, University of Oxford, Parks Road, Oxford OX1 3PH, United Kingdom

[2]Department of Physics and Center for 2 Dimensional and Layered Materials, The Pennsylvania State University, University Park, PA 16802, USA

[3]Department of Engineering Science, University of Oxford, Parks Road, Oxford OX1 3PJ, United Kingdom

[4]Department of Chemistry and Department of Materials Science & Engineering, The Pennsylvania State University, University Park, PA 16802, USA

*Jamie.warner@materials.ox.ac.uk;

Supplementary Figures

Figure S1. Identification of monolayer and bilayer WS_2

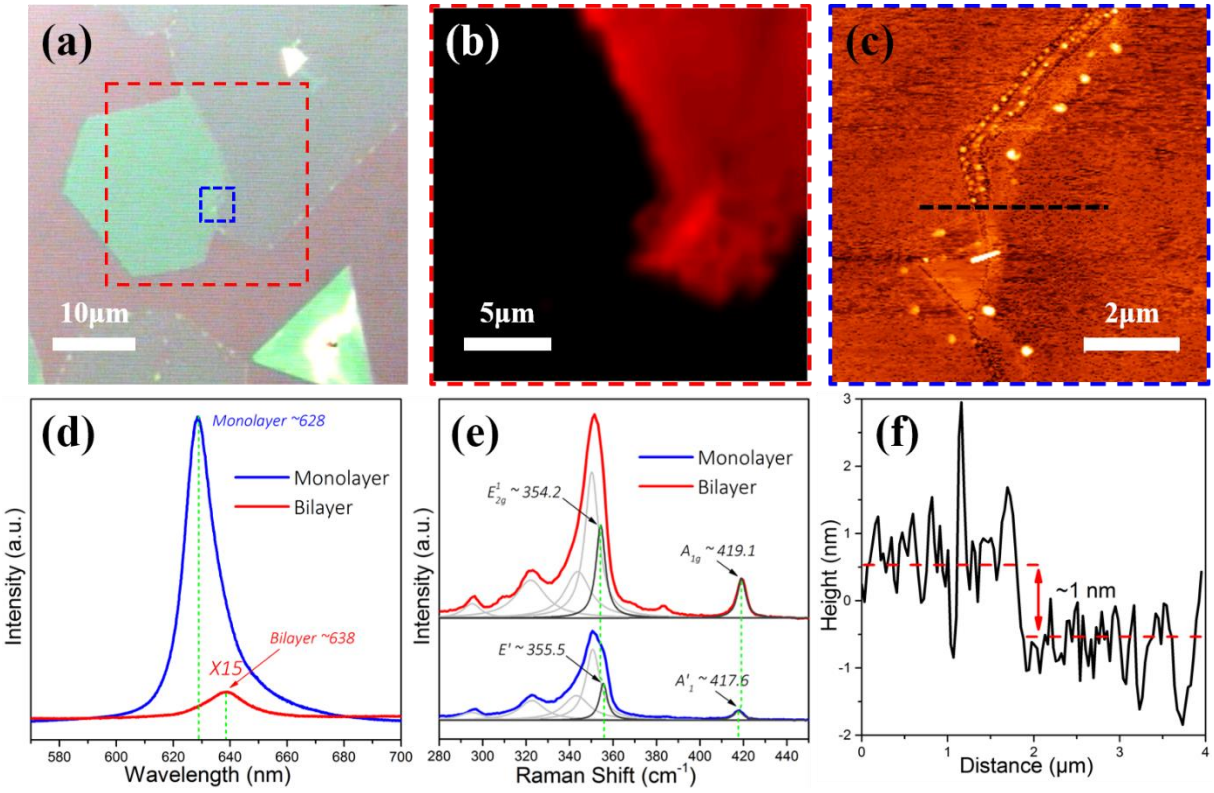

Figure S1. Identification of monolayer and bilayer WS_2. (a) Optical image of an area covered with both bilayer and monolayer WS_2. Light pink is the bare substrate and light green represents monolayer WS_2. Scale bar: 10 μm. (b) PL mapping obtained from the red dashed region in (a). Scale bar: 5 μm. (c) AFM topological mapping of the blue dashed square in (a). Scale bar: 2 μm. (d) PL and (e) Raman spectra of monolayer (blue line) and bilayer (red line) WS_2 on SiO_2/Si, respectively. (f) Corresponding height profile taken across the black dashed line in (c).

Figure S1(a) presents a region covered by both bilayer and monolayer WS_2. Figures S1(c) and (f) give an AFM measurement of the blue dashed region in Figure S1(a), showing the thickness between monolayer and bilayer WS_2 is ~1.0 nm, indicating the capability of

thickness measurement in nanoscale. As can be seen from Figure S1(d), under the same excitation laser power and CCD acquisition time, the PL intensity from the monolayer is about 150 times stronger than that from the bilayer region, due to the emergence of indirect band gap transitions in bilayer WS_2 and the direct band gap transition for monolayer WS_2. There is a 10 nm redshift of the PL Peak position found for bilayer WS_2 compared with monolayer sample, which is in agreement with other literature results.[1–4] Figure S1(b) is the PL mapping of the red dashed area in Figure S1(a), confirming that integrated intensity of monolayer WS_2 is much stronger than that obtained from bilayer. Raman spectroscopy can also help in determining monolayer from bilayer, as shown in Figure S1(e). The blue line represents the Raman spectrum from monolayer WS_2. Curve fitting using multiple Lorentzian distributions was performed to extract the peak positions at 355.5 and 417.6 cm^{-1} in single-layer WS_2 for in-plane (E') and out-of-plane vibration mode (A_1') modes, respectively. Bilayer WS_2 has a slightly different Raman spectrum (red line), with in-plane vibration mode (E^1_{2g}) blue-shifting to 354.2 cm^{-1} and out-of-plane vibration mode (A_{1g}) red-shifting to 419.1 cm^{-1}, consistent with our previously reported literatures.[5]

Figure S2. Optical images of WS_2 shape distribution

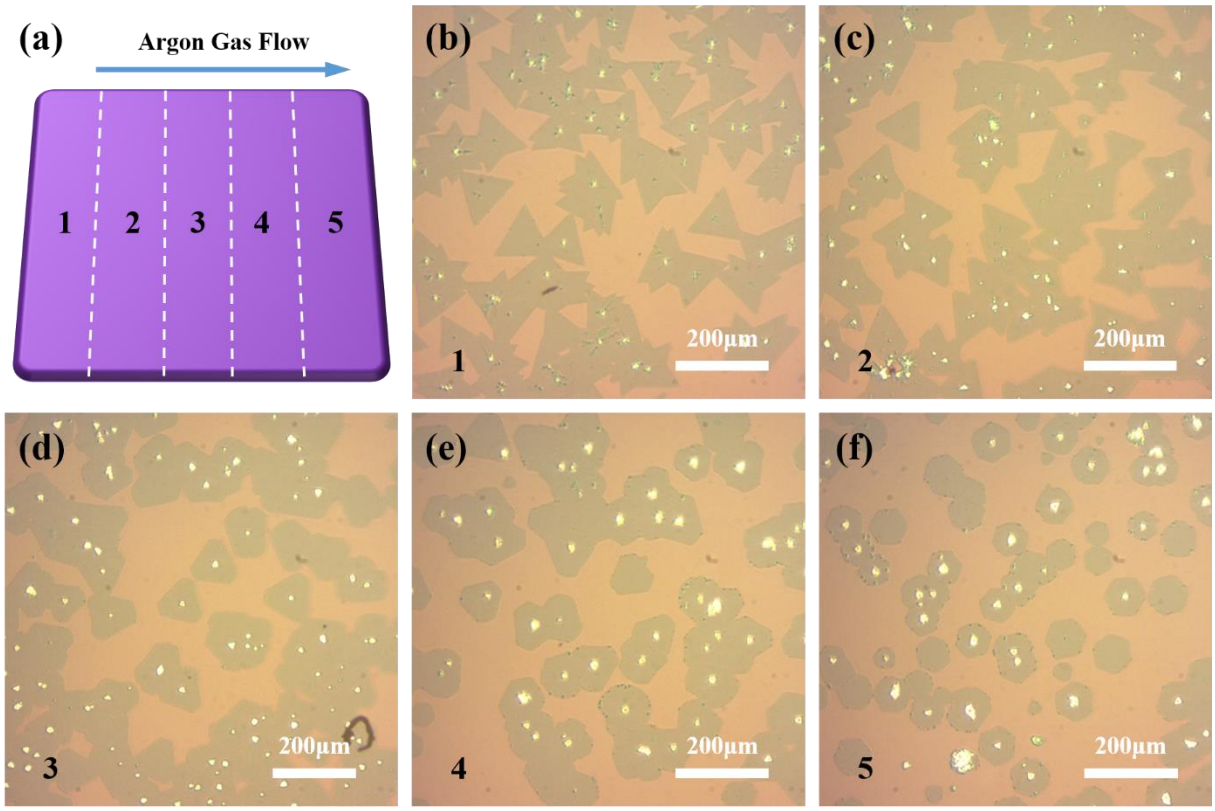

Figure S2. Optical images of WS_2 shape distribution. (a) Schematic illustration showing the spatial sectioning of the growth substrate into five sections along the gas flow direction. The size of the substrate is 2 by 2 cm. (b-f) The corresponding optical images from the center of each section, respectively. Each section of sections 2−4 has a width of 2−3 mm, while sections 1 and 5 have a width of ~5 mm. Scale bar: 200 μm.

Figure S3. Optical images of monolayer WS_2 in different shapes

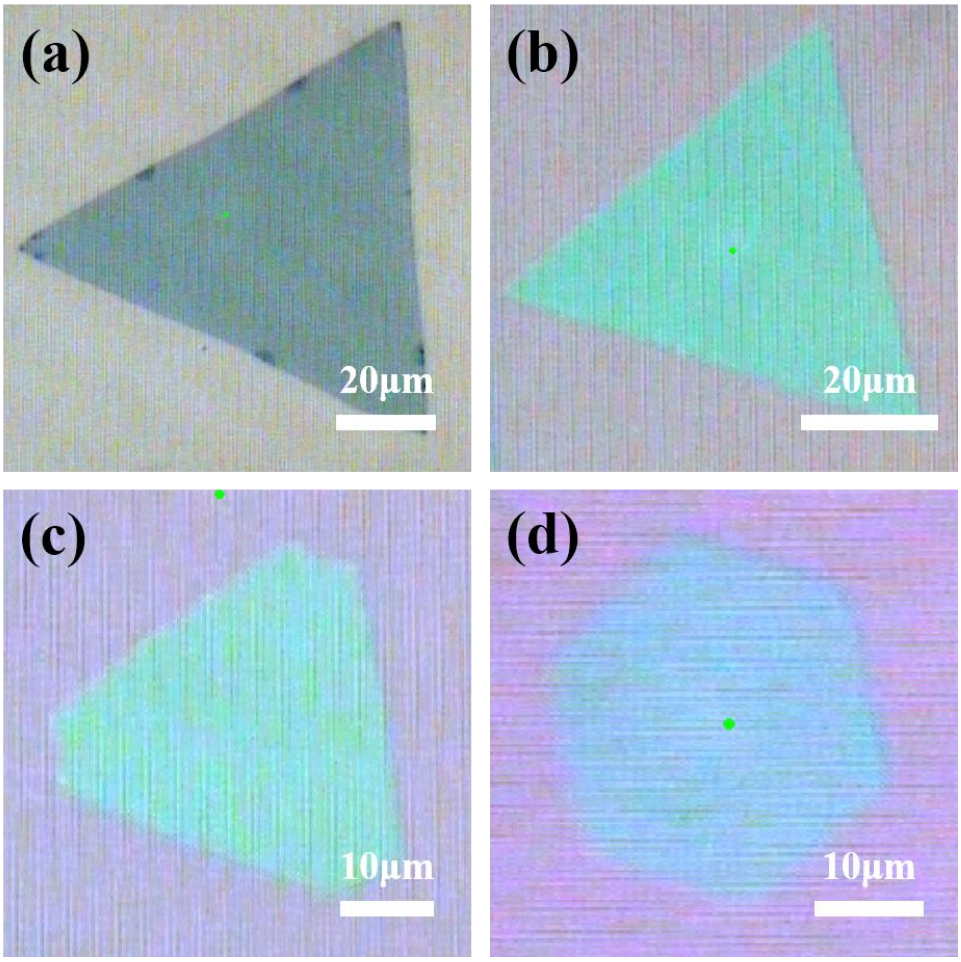

Figure S3. Optical images of monolayer WS_2 in different shapes. (a) Triangle (uniform). Scale bar: 20 μm. (b) Triangle (edge enhanced). Scale bar: 20 μm. (c) Truncated triangle. Scale bar: 10 μm. (d) Hexagon. Scale bar: 10 μm. Two of them were grown on Si substrate with 90 nm SiO_2, while the other two were grown on 300 nm SiO_2.

Figure S3 presents the optical images of monolayer WS_2 in different shapes. They all look very uniform under optical microscope and the contrast indicates monolayer WS_2 according to PL measurement.

Figure S4. Characterization of monolayer WS_2 with symmetric multilayer stacking

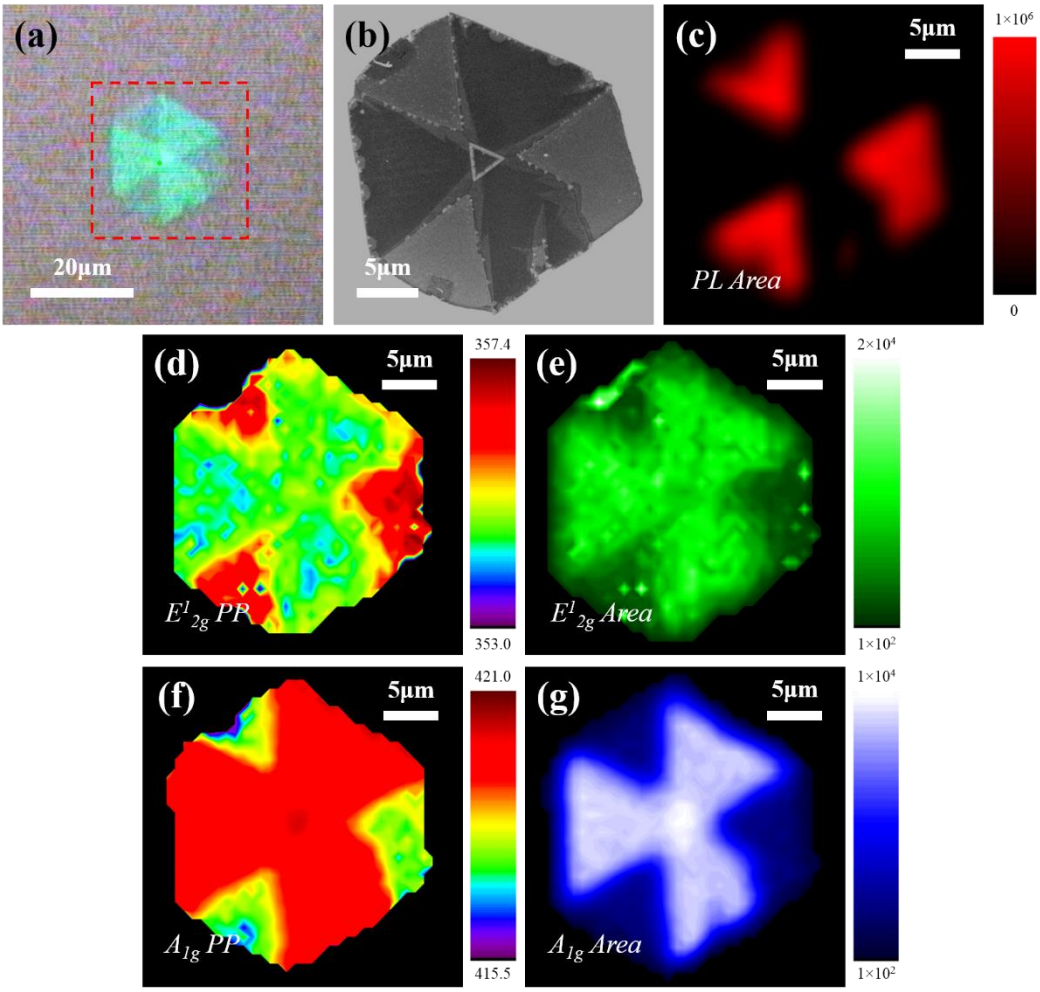

Figure S4. Raman and PL mapping of hexagonal monolayer WS_2 with symmetric multilayer stacking. (a) Optical image of hexagonal monolayer WS_2 crystal with multilayer stacking. Scale bar: 20 μm. (b) SEM image of the same crystal in (a). Scale bar: 5 μm. (c-g) PL and Raman mapping obtained from the red dashed square shown in (a), showing (c) PL integrated intensity, (d) E^1_{2g} peak position and (e) integrated intensity as well as (f) A_{1g} peak position and (g) integrated intensity respectively, indicating obvious distinction between monolayer and few-layer WS_2. Scale bar: 5 μm.

Figure S5. PL mappings of hexagonal WS_2 at different rotation angles

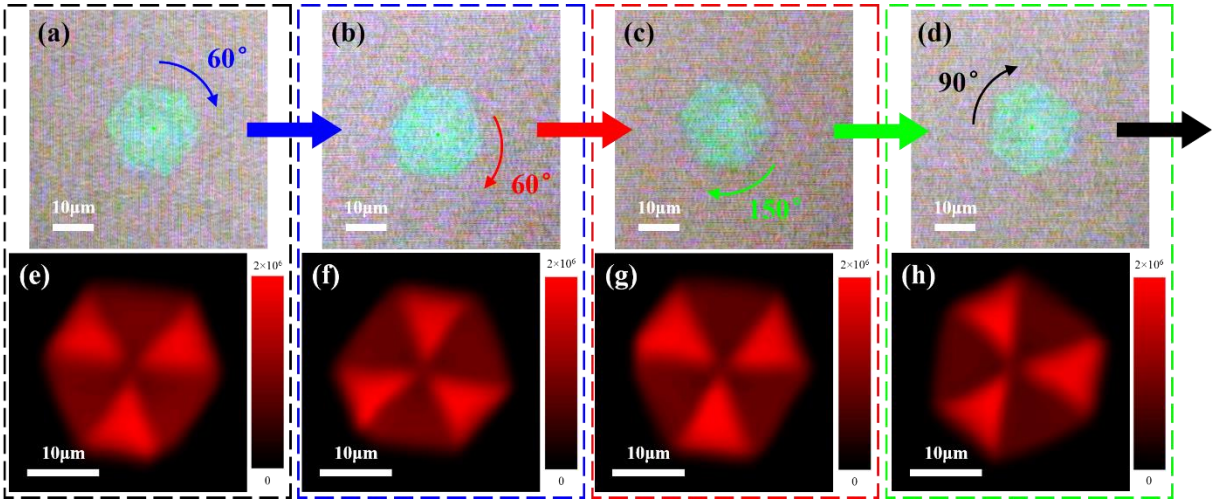

Figure S5. PL mappings and optical images of one typical monolayer hexagonal WS_2 at different rotation angles. (a-d) Optical images of one typical monolayer hexagonal WS_2 domain at rotation angles of 0° (Blue), 60° (Red), 120° (Green) and 270° (Black), respectively. Scale bar: 10 μm. (e-h) The corresponding PL mappings of the same hexagonal WS_2 crystal, showing the same symmetric patterns at different rotation angles. Scale bar: 10 μm.

Figure S6. Optical and SEM images of degraded WS_2 crystal

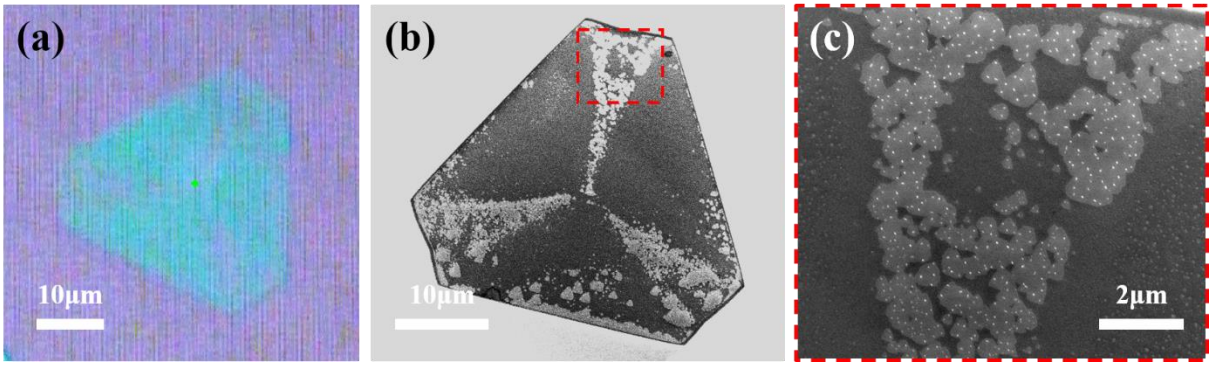

Figure S6. (a, b) Optical and SEM images of the degraded WS_2 crystal on SiO_2/Si substrate. Scale bar: 10 μm. (c) Zoomed-in SEM image of the red dashed area in (b). Scale bar: 2 μm.

Figures S6(a) and (b) present the optical and SEM images of the degraded WS_2 crystal, respectively. Figure S6(c) show the zoomed-in SEM image of the red dashed area in Figure S6(b), indicating the degraded part was formed by small triangles.

Supplementary Tables

Table S1. Lorentzian curve fitting results of the PL spectra taken from six marked spots in hexagonal monolayer WS_2 as shown in Figure 1(d)

Region	Exciton (A)		Trion (A^-)		A/A^-
	PP (eV)	Area (a.u.)	PP (eV)	Area (a.u.)	
i	1.976	239763.9	1.957	138133.6	1.74
ii	1.975	115114.5	1.956	60897.5	1.89
iii	1.976	238423.7	1.957	140323.2	1.70
iv	1.975	106245.1	1.956	52738.5	2.01
v	1.976	236639.7	1.957	137155.7	1.73
vi	1.976	118042.0	1.956	60706.5	1.94
Average (i, iii, v)	1.976	238275.8	1.957	138537.5	1.72
Stdev (i, iii, v)	0.000	1567.4	0.000	1621.9	0.02
Average (ii, iv, vi)	1.975	113133.9	1.956	58114.2	1.95
Stdev (ii, iv, vi)	0.000	6142.8	0.000	4656.5	0.06

Table S2. Lorentzian curve fitting results of the Raman spectra taken from six marked spots in hexagonal monolayer WS_2 as shown in Figure 2(c)

Region	E’		A'_1	
	PP (cm^{-1})	Area (a.u.)	PP (cm^{-1})	Area (a.u.)
i	354.1	27638.2	415.1	10159.3
ii	353.8	26223.6	415.0	12213.4
iii	353.9	31013.5	415.2	9808.1
iv	353.7	25980.8	415.0	9721.1
v	354.0	30174.4	415.2	9825.7
vi	353.6	23899.0	415.5	9998.0
Average (i, iii, v)	354.0	29608.7	415.2	9931.0
Stdev (i, iii, v)	0.1	1757.3	0.0	197.9
Average (ii, iv, vi)	353.7	25367.8	415.2	10644.2
Stdev (ii, iv, vi)	0.1	1277.8	0.3	1366.0

Table S3. Lorentzian curve fitting results of the PL spectra taken from six marked spots in transferred hexagonal monolayer WS_2 as shown in Figure 3(b)

Region	Exciton (A)		Trion (A^-)		A/A^-
	PP (eV)	Area (a.u.)	PP (eV)	Area (a.u.)	
i	2.016	46887.3	1.976	81016.8	0.58
ii	2.016	43113.6	1.976	65163.0	0.66
iii	2.014	45577.3	1.974	79973.7	0.57
iv	2.014	47783.4	1.974	61335.7	0.78
v	2.016	47494.3	1.973	73174.7	0.65
vi	2.015	39161.9	1.973	60900.1	0.64
Average (i, iii, v)	2.015	46653.0	1.974	78055.1	0.60
Stdev (i, iii, v)	0.001	979.8	0.001	4258.6	0.04
Average (ii, iv, vi)	2.015	43352.9	1.974	62466.3	0.69
Stdev (ii, iv, vi)	0.001	4315.7	0.002	2345.6	0.07

Table S4. Lorentzian curve fitting results of the PL spectra taken from the marked spots in a typical hexagonal monolayer WS_2 crystal before and after treatment as shown in Figures 5(b) and (h) respectively

Before Treatment					
Region	Exciton (A)		Trion (A^-)		A/A^-
	PP (eV)	Area (a.u.)	PP (eV)	Area (a.u.)	
i	1.978	38840.0	1.960	18800.0	2.07
ii	1.976	14356.0	1.951	5193.4	2.76
iii	1.977	37117.0	1.957	20273.0	1.83
iv	1.975	14939.0	1.951	5068.0	2.95
v	1.977	28999.0	1.956	15184.0	1.91
vi	1.976	14330.0	1.950	4838.9	2.96
Average (i, iii, v)	1.977	34985.3	1.958	18085.7	1.94
Stdev (i, iii, v)	0.001	5255.4	0.002	2618.6	0.12
Average (ii, iv, vi)	1.976	14541.7	1.951	5033.4	2.89
Stdev (ii, iv, vi)	0.001	344.3	0.001	179.8	0.11
After Treatment					
i’	1.973	20566.0	1.958	15297.0	1.34
ii’	1.969	12098.0	1.950	7668.7	1.58
iii’	1.973	15907.0	1.957	11472.0	1.39
iv’	1.970	11867.0	1.951	6847.7	1.73
v’	1.972	17681.0	1.953	12757.0	1.39
vi’	1.968	11642.0	1.949	7301.2	1.59
Average (i’, iii’, v’)	1.973	18051.3	1.956	13175.3	1.37
Stdev (i’, iii’, v’)	0.001	2351.5	0.003	1946.5	0.02
Average (ii’, iv’, vi’)	1.969	11869.0	1.950	7272.5	1.64
Stdev (ii’, iv’, vi’)	0.001	228.0	0.001	411.3	0.09

Reference

(1) Zeng, H.; Liu, G.-B.; Dai, J.; Yan, Y.; Zhu, B.; He, R.; Xie, L.; Xu, S.; Chen, X.; Yao, W.; Cui, X. Optical Signature of Symmetry Variations and Spin-Valley Coupling in Atomically Thin Tungsten Dichalcogenides. *Sci. Rep.* **2013**, *3*, 1608.

(2) Gutiérrez, H. R.; Perea-López, N.; Elías, A. L.; Berkdemir, A.; Wang, B.; Lv, R.; López-Urías, F.; Crespi, V. H.; Terrones, H.; Terrones, M. Extraordinary Room-Temperature Photoluminescence in Triangular WS_2 Monolayers. *Nano Lett.* **2013**, *13*, 3447–3454.

(3) Zhao, W.; Ghorannevis, Z.; Chu, L.; Toh, M.; Kloc, C.; Tan, P.; Eda, G. Evolution of Electronic Structure in Atomically Thin Sheets of WS_2 and WSe_2. *ACS Nano* **2013**, *7*, 791–797.

(4) He, Z.; Xu, W.; Zhou, Y.; Wang, X.; Sheng, Y.; Rong, Y.; Guo, S.; Zhang, J.; Smith, J. M.; Warner, J. H. Biexciton Formation in Bilayer Tungsten Disulfide. *ACS Nano* **2016**, *10*, 2176–2183.

(5) He, Z.; Sheng, Y.; Rong, Y.; Lee, G.; Li, J.; Warner, J. H. Layer-Dependent Modulation of Tungsten Disulfide Photoluminescence by Lateral Electric Fields. *ACS Nano* **2015**, *9*, 2740–2748.